

CLASSIFICATION OF LAYERED TISSUE PHANTOMS FOR DETECTION OF CHANGES IN EPITHELIAL TISSUE BELOW THE SURFACE USING A STOCHASTIC DECOMPOSITION MODEL FOR SCATTERED SIGNAL

Fernand S. Cohen, Ezgi Taslidere*, and, Sreekant Murthy***

**Department of Electrical and Computer Engineering*

*** Division of Gastroenterology and Hepatology, College of Medicine
Drexel University, Philadelphia, PA 19104*

ABSTRACT

This paper answers the question of whether it is possible to detect changes inside epithelium layered structures using a Stochastic Decomposition Method (SDM) [1, 2] that models the scattered light reflected from the layered structure over an area (2-D scan) illuminated by an optical sensor (fiber) emitting light at either one wavelength or with white light. Our technique correlates the differential changes in the reflected tissue texture with the morphological and physical changes that occur in the tissue occurring below the surface of the structure. This work has great potential in detecting changes in mucosal structures and may lead to enhanced endoscopy when the disease is developing to the below the surface and hence becoming hidden during colonoscopy or endoscopic examination. Tests are performed on layered tissue phantoms and the results obtained show great effectiveness of the model and method in picking up changes in the morphology of the layered tissue phantoms occurring below the surface (greater than 0.6mm deep).

Index Terms— biomedical signal analysis, optical imaging, optical signal processing, spectral analysis, stochastic processes.

1. INTRODUCTION

Various optical techniques have been developed for early diagnosis of epithelial cancer. Detailed reviews of these available optical techniques are presented in the literature with analysis of their advantages and disadvantages [3]. The motivation behind using the optical based techniques is that for the cases of malignancy detected at an earlier stage in colorectal cancer, a 5-year survival in excess of 97% can occur [4]. In recent years considerable progress has been made to evaluate subsurface structures in biological tissues *in vivo*. Confocal laser endomicroscopy, which is the closest step towards virtual histology has lead to the evaluation of the whole mucosal layer with an infiltration depth up to 250 μm [5]. Likewise, confocal fluorescence endomicroscopy may have the capacity to reach to 15-100 μm depth of penetration [6]. While those techniques use fluorescent dyes to interrogate subsurface information, other researchers are focusing on extracting information from tissue layers at different depths using reflected light [7, 8] without the use of dyes. Thus, the ultimate goal is to detect changes in the sub-epithelial tissue since early cancer development might occur at this level, hence attention needs to be focused on detection of morphological changes below the surface [9]. In this paper we aim

to differentiate different tissue morphologies below tissue surface. We have previously presented a Stochastic Decomposition Method (SDM) model as a plausible model for mucosal tissues [1, 2]. We tested the performance of the model, i.e., its ability to differentiate different tissue characteristics using simulations and phantom data that were designed to mimic dysplasia formation. The reported results verified the applicability of the model for differentiation of different tissue characteristics [1, 2]. In order to test the sensitivity of the model and method to changes occurring below the surface of the tissue, we use doubly layered mimicking tissue phantoms representing different tissue morphologies at different depths below the surface. Our data demonstrates that our SDM model is capable of discriminating tissue changes reliably and reproducibly below the epithelial surface.

2. BIOLOGICAL MOTIVATION

Our depth sensitivity analysis is motivated by the biological problem of cancer formation in mucosal tissue in the colon from scattered light. Human colon is composed of four layers mucosa, submucosa, muscularis externa propria and serosa; a schematic representation is given in Figure 1 [7]. The light incident on the colon surface first interacts with the thin epithelium layer and then gets transmitted through the first layer into deeper layers [7]. The reflected light due to the epithelium layer (outer layer) is 2-5% of the total reflected light [10]. Hence, the scattered light carries information from layers below the surface. Early colorectal cancer are classified as protruded, superficial elevated, flat, and depressed type [11]. Detection of flat and depressed lesions is quite difficult during endoscopy [12]. Depressed lesions have high risk of submucosal invasion [5]. The average thickness of mucosal layer is approximately 400 μm [13], and varies in the range 395-603 μm [7]. Since most biological tissues have a multilayered structure, depth-resolved measurements are important [14].

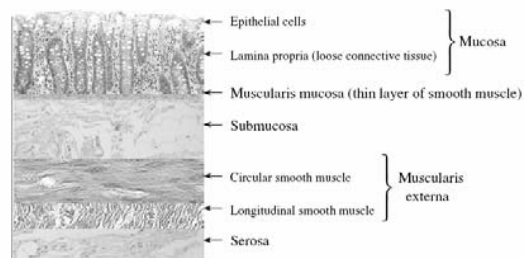


Fig. 1. Schematic representation of colon architecture [7].

3. CLASSIFICATION OF LAYERED TISSUE PHANTOMS

Here we answer the question of whether or not the SDM and its parameters are sensitive to phantom structure changes, when the changes occur below the surface (greater than 0.6mm) of the phantom structure. We consider the parameters extracted from the SDM at one wavelength, plus the parametric power spectral density (PSD) that is formed based on these estimated SDM parameters, and proceed to establish whether or not such sensitivity exists based on multi-layered designed phantoms. We also generalize the analysis to include the white light case.

3.1. The Diffuse Model

The SDM model [1, 2] uses reflected light at one specific wavelength λ . SDM method is based on the idea that any regular process $y(n)$ can be expressed as a sum of diffuse ($d(n)$) and specular ($c(n)$) components. For a totally diffuse component $d(n)$ (which is the case considered in this paper) is a zero mean autoregressive process of order p ($AR(p)$) process

$$d(n) = \sum_{s=1}^p b_s d(n-s) + w(n) \quad (1)$$

The AR process is the output of a linear filter $H(f, \lambda)$

$$H(f, \lambda) = \frac{1}{(1 - \sum_k b_k(\lambda) e^{-j2\pi f k})} \quad (2)$$

which is driven by zero mean white noise sequence $w(n)$ with variance $\sigma^2(\lambda)$. The AR process is parameterized by the set $(b_1(\lambda), b_2(\lambda), \dots, b_p(\lambda), \sigma^2(\lambda)) = (\mathbf{b}(\lambda), \sigma^2(\lambda))$. $\mathbf{b}(\lambda)$ describes the correlation structure (texture) between the points in the data, whereas $\sigma^2(\lambda)$ conveys information about the strength (intensity) of the driving noise. The Parametric Power Spectral Density (PSD) is defined as:

$$S(f, \lambda) = |H(f, \lambda)|^2 \sigma^2(\lambda) \quad (3)$$

To limit the PSD to strictly conveying changes due to texture information alone we can normalize the PSD so that the $AR(p)$ process under any structure is having $\sigma^2(\lambda) = 1$. This is done by taking the normalized PSD as $\hat{S}(f, \lambda) = S(f, \lambda) / \sigma^2(\lambda)$. In addition to $\sigma^2(\lambda)$ and $\hat{S}(f, \lambda)$, we also consider the Kolmogorov-Smirnov (KS) distance $D(\lambda)$ [1, 2].

3.2. Metric Based on the AR Parameters for Testing whether or not Two Structures Are Similar or Different

We want to test whether two layered tissue structures, denoted here by A and B, and which are interrogated at a wavelength λ , are deemed to be the same (i.e., $H_o: A = B$, where H_o is the null hypothesis) or different (i.e., $H_a: A \neq B$, where H_a is the alternative hypothesis), based on two A-scans (see section 4.1 for how the data is collected to form a 1-D signal or A-scan). The estimated $AR(p)$ parameters obtained from the two A-scans are γ_A and γ_B . Towards that end we use the following metric statistics

$$d_{s,\lambda} = \frac{\gamma_A(\lambda) - \gamma_B(\lambda)}{\gamma_A(\lambda) + \gamma_B(\lambda)} \quad (4)$$

The metric $|d_{s,\lambda}|$ is bound between 0 and 1, where it assumes the value 0 when $\gamma_f(A) = \gamma_f(B)$, and assumes the maximum value of 1 when either $\gamma_f(A) = 0$ or $\gamma_f(B) = 0$. Finally, if we consider the entire white light spectrum instead of just one wavelength, we should expect better performance since different wavelengths have

different penetration, with larger wavelengths are expected to give a higher performance as they penetrate deeper in the tissue. Of course, this also depends on the scattering/absorption coefficient of the tissue. If the coefficient is really high, then the signal will be so attenuated that the reflected intensity will be so weak.

For the white light case the metric for $\sigma^2(\lambda)$ and $D(\lambda)$ become $d_{s,\lambda}$ (Eq. 5) evaluated at $\lambda_{\max}: d_{s,\lambda}(\lambda_{\max})$, where λ_{\max} is the wavelength at which $|d_{s,\lambda}|$ assumes its maximum value; and for the normalized spectrum $\hat{S}(f, \lambda)$ it is

$$d_{s,\lambda} = \frac{\hat{S}_A(f_{\max}, \lambda_{\max}) - \hat{S}_B(f_{\max}, \lambda_{\max})}{\hat{S}_A(f_{\max}, \lambda_{\max}) + \hat{S}_B(f_{\max}, \lambda_{\max})} \quad (5)$$

where f_{\max} and λ_{\max} are the frequency and wavelength pair at which $|d_{s,\lambda}|$ assumes its maximum value. When $|d_{s,\lambda}|$ is close to 0, then this will support the hypothesis that the two structures are seen as basically the same based on the data examined, whereas $|d_{s,\lambda}|$ values away from 0, would support the hypothesis that the structures are judged to be different. Remember that in the context of our problem, structures A and B only differ in their deeper (below the surface) layers, but are the same on the outer layers. So when we judge them to be different, in essence we are saying that the parameters are sensitive to changes in the deeper layers. Finally, it is important to establish what constitutes legitimate “away from 0” values and ways of establishing it. $d_{s,\lambda}$ is a statistic (a random variable) that is based on estimated parameters from finite data (the reflected intensity over a scan). It has a mean value $E[d_{s,\lambda}]$ and a standard deviation $STD[d_{s,\lambda}]$. Under $H_o: A = B$, $E[d_{s,\lambda} | H_o] = 0$, and a nonzero standard deviation $\sigma_d = STD[d_{s,\lambda} | H_o]$ which goes to zero as the record size of the A-scan gets larger and larger. Given an A-scan from a test structure (say structure B) and an A-scan from a nominal structure (say structure A), we estimate the test and nominal structure parameters from that two A-scans, and for each one of the parameters compute the $d_{s,\lambda}$ metric. Then we compare $d_{s,\lambda}$ to σ_d , and if $|d_{s,\lambda}| < 2\sigma_d$, we declare the two structures to be the same (i.e., $A = B$), otherwise we declare them to be different (i.e., $A \neq B$). The threshold $2\sigma_d$ results in a very conservative classification rule, where two structures are deemed different if there is so much evidence that the two models estimated from the nominal and test data are very different. To make the decision independent of which structure is considered as the nominal, the classification rule is compared to the largest of $\sigma_{d,A}$ and $\sigma_{d,B}$, where $\sigma_{d,A}$ is the sample standard deviation for $d_{s,\lambda}$ when A is considered as the nominal structure, and $\sigma_{d,B}$ is for when B is considered as the nominal structure.

We determine an approximate value for σ_d using Monte Carlo simulations as follows. Given an A-scan from a nominal structure (taken as either structure A or structure B), we estimate the $AR(p)$ parameters, then we generate Monte Carlo realizations in accordance with the estimated $AR(p)$ parameters. For each such realization, we re-estimate the parameters. For each one of the parameters, we compute the corresponding sample $d_{s,\lambda}$. Out of all the $d_{s,\lambda}$ samples for that parameter, the sample standard deviation σ_d is computed. This constitutes the nominal sample standard deviation for the metric under the nominal structure (i.e., when H_o is in effect) which under white light will be an upper bound for σ_d

over all λ 's when the metric $d_{s,\lambda}$ is constructed based on either $\sigma^2(\lambda)$ or $D(\lambda)$, and over all λ 's and f 's when the metric $d_{s,\lambda}$ is constructed based on $\hat{S}(f, \lambda)$.

3.3. Multi Looks- Multi Scans Case

When multiple A-scans are available, then an alternative metric to $d_{s,\lambda}$, which is based on the estimated histograms associated with each of the parameters under structures A and B can be computed. From these two histograms one can construct an ROC and use the area A_z under the ROC curve as a measure of the ability of that parameter to discriminate between structures A and B based on changes in the inner layer (deep under the surface). This measure has been used in our work in [1, 2] to differentiate between one layer structures. Details on the calculation of A_z are given in [1, 2]. We report on the performance of the single parameters $\sigma^2(\lambda)$ and $D(\lambda)$ using a permutation method that creates additional virtual A-scans from the observed original one. Since these two parameters are not affected by the data order, data permutation is kosher. This is not the case; however, with regards to the parameter $\hat{S}(f, \lambda)$ as the correlation structure (the texture) is affected by data permutation.

4. PERFORMANCE EVALUATION ON LAYERED TISSUE PHANTOMS

4.1. Specifications of Layered Phantoms and Data Collection

The layered tissue phantoms are created [15] using different sizes of polystyrene latex micro spheres (Polysciences Inc). We examined micro spheres at diameter sizes of $2\mu m$, $3\mu m$, $4\mu m$ and $10\mu m$. A gelatin layer is placed in between two types of micro spheres of different sizes. The heights of the top and bottom layer tissue phantom are approximately 0.6mm each, and the height of gelatin layer in the middle is around 0.4mm. The details of specifications and creation of layered tissue phantoms are given in [15]. We name the samples as N1N2, where N1 is microsphere size (in microns) at the bottom layer and N2 is the microsphere size at the top layer. A sample structure of the layered tissue phantoms are given in Figure 2.

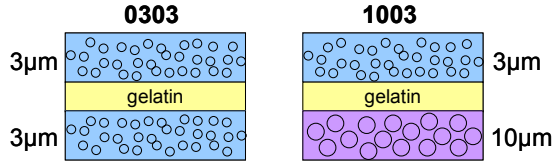


Fig. 2. The structure of layered tissue phantoms for samples 0303 and 0310.

Phantom data is collected using a probe, a spectrometer, and a light source [16]. The sample is illuminated with white-light and the reflected light intensities over the white spectrum is collected at equal spaced intervals during scanning, using a staging station. The details of data collection is explained in our previous work [2]. To create an A-scan, the fiber is placed on a XYZ stage, which moves the fiber and allows data to be collected at different points on the sample. If there are M (for the spectrometer used there were 1243 values extending the range of 400-800nm) numbers of wavelengths that we consider over the white spectrum, then there are M numbers of A-scans that are considered, one at each wavelength, for each of which the $AR(p)$ parameters are extracted.

4.2. Performance Evaluation of the Model Parameters based on the Distance Metric over the White Spectrum

In this section we report on the ability of the model parameters $D(\lambda)$, $\sigma^2(\lambda)$, and $\hat{S}(f, \lambda)$ to differentiate between pairs of phantom structures that only differ in their lower layers (i.e., the upper layers for the two structures are the same as shown in Figure 2 over the entire white spectrum using the distance metric introduced in Section 3.2. The pairs of structures considered are 0202-0402, 0404-0204, 0303-1003, and 1010-0310. For each one of the 8 structures considered, the standard deviations (σ_d 's) of ($d_{s,\lambda}$)'s under each structure are computed from 1000 Monte Carlo realizations for each structure (see Section 3.2) based on the $AR(p)$ (with p set to 5) parameters that are estimated from the A-scan associated with that structure. For each realization, the model parameters are extracted and the distance metric $d_{s,\lambda}$ for each of

the extracted parameters $D(\lambda)$, $\sigma^2(\lambda)$, and $\hat{S}(f, \lambda)$ are calculated in order to obtain the standard deviations (σ_d 's). The performance of the distance metric as a function of σ_d 's for $D(\lambda_{\max})$, $\sigma^2(\lambda_{\max})$, and $\hat{S}(f_{\max}, \lambda_{\max})$ are given in Table 1. As we can see from the table, all but one value is below the $2\sigma_d$ threshold (the structure pair 0303-1003 for the metric based on $\hat{S}(f_{\max}, \lambda_{\max})$ parameter, which is barely below the $2\sigma_d$ threshold ($1.9573 \sigma_d$)). This implies that for all the cases, the pairs are classified as different based on any one the single model parameters. It is also interesting to observe how far away the $d_{s,\lambda}$ values are from the $2\sigma_d$ threshold for the $D(\lambda_{\max})$ and $\sigma^2(\lambda_{\max})$ parameters. If we combine the classification based on individual parameters, the combined distance will be very far away from the $2\sigma_d$ threshold for all cases. On overall, the model parameters are able to strongly discriminate between structures differing only in their lower layers.

Table 1. The metric $d_{s,\lambda}(\sigma_d)$ for the features.

$d_{s,\lambda}(\sigma_d)$	$D(\lambda_{\max})$	$\sigma^2(\lambda_{\max})$	$\hat{S}(f_{\max}, \lambda_{\max})$
0202-0402	$13.539 \sigma_d$	$11.725 \sigma_d$	$2.0573 \sigma_d$
0404-0204	$4.576 \sigma_d$	$17.314 \sigma_d$	$2.2963 \sigma_d$
0303-1003	$5.242 \sigma_d$	$31.770 \sigma_d$	$1.9573 \sigma_d$
1010-0310	$4.162 \sigma_d$	$22.577 \sigma_d$	$2.1694 \sigma_d$

4.3. Performance Evaluation based on the Distance Metric for Multi Scans as Area under ROC curves

In this section, we report on the performance of $D(\lambda)$ and $\sigma^2(\lambda)$, using the permutation method and A_z described in Section 3.3. From an A-scan at given λ , we generate additional 99 A-scans using permutations. From these 100 A-scans, 100 values for $\sigma^2(\lambda)$, and $D(\lambda)$ are computed for that given structure at that particular wavelength, and a pair of histograms, one for the $\sigma^2(\lambda)$ parameter, and one for the $D(\lambda)$ parameter, are generated. This process is repeated for all 1243 additional wavelengths associated with the white spectrum. When testing a pair of structures that only differ in their lower layers, the histograms for $D(\lambda)$ and $\sigma^2(\lambda)$ at the interrogating wavelength are used to compute the A_z for that wavelength. For the white light spectrum there will be 1243 possible A_z values for that pair of structures. We report the mean value of these A_z 's in Table 2 for each of the parameters. We also report on the performance when

we optimally combine the two parameters together in accordance with the joint likelihood ratio statistics (Neyman Pearson statistics) [1, 2]. As we can see from Table 2, the performance is extremely strong (A_z value close to 1) for the individual parameters in particular for the $\sigma^2(\lambda)$ parameter. The results of classification by fusing all the imaging parameter set together yields an overall extremely strong performance (A_z between 0.980-1.000), showing that changes in the lower layer of the layered tissue phantoms are reliably detected using the model and method.

Table 5. Mean A_z values for classification for pairs of layered phantoms for parameters $D(\lambda)$, $\sigma^2(\lambda)$.

A_z for D	A_z for D	A_z for σ^2	A_z for $D+\sigma^2$
0202-0402	0.9962	0.9804	0.9986
0404-0204	0.9804	0.9800	1.0000
0303-1003	0.9793	0.9804	0.9997
1010-0310	0.8790	0.9801	1.0000

6. CONCLUSION

We investigated the ability of our SDM model [1, 2] and its parameters in detecting structure changes below the surface by comparing between phantoms that had similar structures on their upper layers, but different structures in their lower layers. This study was motivated by the biological problem of cancer formation in mucosal tissue in the colon from scattered light, for potential detection of early cancer development where morphological changes usually occur below the surface. Our technique correlates the differential changes in the reflected tissue texture with the morphological and physical changes that occur in the tissue occurring below the surface of the structure. Methodologies are developed for judging the sensitivity of the texture model parameters to changes occurring deep inside the structures (greater than 0.6mm deep) from A-scans obtained over one wavelength within the white light range (400-800nm). The performance of these parameters is shown to be extremely strong as reflected by either one of the two metrics considered, $d_{s,\lambda}$ or A_z .

For all pairs of phantom structures considered with structure differences in their lower layers only, the distance metric $d_{s,\lambda}$ had values well exceeding the $2\sigma_d$ high threshold for all but one value for the structure pair, which is barely below the $2\sigma_d$ threshold ($1.9573\sigma_d$). This finding is also collaborated by the extremely high values obtained using the second metric A_z which returned almost perfect classification values (0.98-1.00) when discriminating between pairs of tissue mimicking phantoms that had different structures only in their lower layers below surface.

7. ACKNOWLEDGEMENTS

We would like to thank Photonics Lab members: Ms. Elina Vitol, Dr. Timothy Kurzweg and Dr. Bahram Nabet in the ECE Dept. at Drexel University for providing the optical device (probe, spectrometer and light source) and the phantoms used in this research. Special thanks are also due Ms. Elina Vitol for preparing the multi-layered tissue phantoms. We also thank Dr. Jim Reynolds from Drexel College of Medicine for many useful discussions on the subject of light endoscopy.

8. REFERENCES

- [1] F. S. Cohen, E. Taslidere, and D. S. Hari, "Tissue characterization and detection of dysplasia using scattered light," in *Biomedical Imaging: Nano to Macro, 2006. 3rd IEEE International Symposium on*, 2006, pp. 590-593.
- [2] E. Taslidere and F. S. Cohen, "Stochastic Decomposition Method for Detection of Epithelium Dysplasia and Inflammation using White Light Spectroscopy Imaging," in *Engineering in Medicine and Biology Society, 2006. EMBS '06. 28th Annual International Conference of the IEEE*, 2006, pp. 1956-1959.
- [3] R. S. Dacosta, B. C. Wilson, and N. E. Marcon, "Spectroscopy and fluorescence in esophageal diseases," *Best Pract Res Clin Gastroenterol*, vol. 20, pp. 41-57, Feb 2006.
- [4] J. Moreaux and M. Catala, "Carcinoma of the Colon - Long-Term Survival and Prognosis after Surgical-Treatment in a Series of 798 Patients," *World Journal of Surgery*, vol. 11, pp. 804-808, Dec 1987.
- [5] R. Kiesslich and M. F. Neurath, "Endoscopic detection of early lower gastrointestinal cancer," *Best Pract Res Clin Gastroenterol*, vol. 19, pp. 941-61, Dec 2005.
- [6] A. Osdoit, F. Lacombe, C. Cavé, S. Loiseau, and E. Peltier, "To see the unseeable: confocal miniprobes for routine microscopic imaging during endoscopy," in *Proc. SPIE 6432, 64320F* 2007.
- [7] D. Hidovic-Rowe and E. Claridge, "Modelling and validation of spectral reflectance for the colon," *Phys Med Biol*, vol. 50, pp. 1071-93, Mar 21 2005.
- [8] Q. Liu and N. Ramanujam, "Sequential estimation of optical properties of a two-layered epithelial tissue model from depth-resolved ultraviolet-visible diffuse reflectance spectra," *Applied Optics*, vol. 45, pp. 4776-4790, Jul 1 2006.
- [9] P. Fockens, "Future developments in endoscopic imaging," *Best Pract Res Clin Gastroenterol*, vol. 16, pp. 999-1012, Dec 2002.
- [10] R. A. Zangaro, L. Silveira, R. Manoharan, G. Zonios, I. Itzkan, R. R. Dasari, J. VanDam, and M. S. Feld, "Rapid multiexcitation fluorescence spectroscopy system for in vivo tissue diagnosis," *Applied Optics*, vol. 35, pp. 5211-5219, Sep 1 1996.
- [11] S. Kudo, H. Kashida, T. Tamura, E. Kogure, Y. Imai, H. Yamano, and A. R. Hart, "Colonoscopic diagnosis and management of nonpolypoid early colorectal cancer," *World Journal of Surgery*, vol. 24, pp. 1081-1090, Sep 2000.
- [12] J. D. Wayne, D. K. Rex, and C. B. Williams, "G. S. Raju and P. J. Pasricha, "Flat and Depressed Colorectal Neoplasia in the Western Hemisphere", in *Colonoscopy : principles and practice*, 1st ed Malden, Mass.: Blackwell, 2003, pp. x, 655 p.
- [13] C. K. Brookner, M. Follen, I. Boiko, J. Galvan, S. Thomsen, A. Malpica, S. Suzuki, R. Lotan, and R. Richards-Kortum, "Autofluorescence patterns in short-term cultures of normal cervical tissue," *Photochemistry and Photobiology*, vol. 71, pp. 730-736, Jun 2000.
- [14] Y. Liu, Y. L. Kim, and V. Backman, "Development of a bioengineered tissue model and its application in the investigation of the depth selectivity of polarization gating," *Applied Optics*, vol. 44, pp. 2288-2299, Apr 20 2005.
- [15] E. A. Vitol, B. Nabet, and T. P. Kurzweg, "Depth Sensitive Fiber Optic Probe for Light Scattering Characterization of a Multilayered Epithelial Tissue Model " *Submitted to Journal of Biomedical Optics*, 2007.
- [16] E. A. Vitol, T. P. Kurzweg, and B. Nabet, "Using white-light spectroscopy for size determination of tissue phantoms," in *Proc. SPIE Photonics North*, Toronto, Canada, 2005.